Journal of Sound and Vibration 432 (2018) 387–404

Contents lists available at ScienceDirect

Journal of Sound and Vibration

journal homepage: www.elsevier.com/locate/jsvi

Modal evaluation and generalized analysis of the steady-state dynamics of harmonically excited multistable structures

Benjamin A. Goodpaster [a], Ricardo A. Perez [b], Ryan L. Harne [a, *]

[a] Department of Mechanical and Aerospace Engineering, The Ohio State University, Columbus, OH, USA
[b] Universal Technology Corporation, Dayton, OH, USA

ARTICLE INFO

Article history:
Received 7 December 2017
Received in revised form 28 April 2018
Accepted 19 June 2018

Handling Editor: Ivana Kovacic

Keywords:
Nonlinear vibration
Multistable structure
Reduced order model
Linearization

ABSTRACT

Predictions of multistable structural dynamics are paramount to the development and deployment of air vehicles operating under extreme loading conditions. Although time-stepping numerical techniques may capture the multi-physics interactions that occur in these environments, the generalized insight on parameters that predominantly govern the system behaviors may remain clouded while a large computational expense may be incurred to obtain response predictions. Alternatively, analytical methods may be employed to streamline the prediction process, yet current theoretical approaches do not facilitate such opportunity for multistable structures. Although a recently developed analytical formulation has enabled the prediction of near- and far-from-equilibrium responses for a simplified multistable structure, the preliminary formulation does not illuminate the underlying aspects of modal response and intricate nonlinear coupling manifest in myriad multistable systems. This research rectifies these limitations by a broad expansion of the analytical framework that empowers a new modal perspective of multistable structural dynamics and enables the study of such dynamic systems governed by reduced order models. This new modal analysis indicates that the characteristic frequency response of a single degree-of-freedom Duffing oscillator is preserved in the fundamental equivalent nonlinear mode of a multistable structure. The new analytical formulation is also shown to accurately predict the near- and far-from-equilibrium dynamics of equation systems containing global nonlinear coupling consistent with reduced order models. The advancements achieved in this work contribute to the suite of techniques available to researchers to characterize the near-to- and far-from equilibrium behaviors of nonlinear dynamic systems consisting of many degrees-of-freedom.

1. Introduction

From sub-orbit flight initiatives [1], to supersonic passenger jets [2], to hypersonic air vehicles [3]: applications abound for high-performance aerospace vehicles operating in extreme environments. Yet, the full realization of such air vehicles is impeded due to the combined thermo-mechanical-acoustical loading of high velocity flight regimes [4] that may stress slender aerostructural components into states of multistability, termed skin-buckling [5]. Once deformed, structural panels may exhibit a large-amplitude, snap-through dynamic response that can accelerate structural damage measures, lower

* Corresponding author.
E-mail address: harne.3@osu.edu (R.L. Harne).

https://doi.org/10.1016/j.jsv.2018.06.049
0022-460X/

fatigue life, and amplify the chances of catastrophic failure [6,7]. To surmount these challenges, recent works by Miller and McNamara [8] and Culler and McNamara [9,10] have advanced simulation of the complex fluid-thermal-structural coupling present for multistable panels in hypersonic flow. Miller et al. [11] gave particular attention to simulate the snap-through phenomenon in a multi-physics load environment. The computational demands encountered in such time-step simulation-based studies have provided motivation for the development of reduced order models (ROMs). ROMs decrease the dimension of the equation system thus lowering computational time, while prediction fidelity is balanced in the process. ROM-based characterizations of multistable structures have been reported by Wiebe and Spottswood [12], Mignolet et al. [13], and Matney et al. [14]. These numerical investigations have delivered new knowledge on the dynamic responses of multistable structures in extreme operating environments. Yet, the insight on such nonlinear structural behavior remains limited through the undertaking of case studies by simulation methods alone.

Analytical methods that approximately solve the governing equations of motion of nonlinear systems may greatly enhance the understanding revealed on the system response by way of meaningful simplifying assumptions [15]. Perturbation techniques can uncover the nonlinear, frequency-dependent displacement amplitudes of intrawell oscillations up to an arbitrary order of the small perturbation parameter ε [16]. Alternative forms of the standard perturbation technique, such as parameter-expanding methods [17,18] and homotopy perturbation [17,19], may be used to study any nonlinear dynamical equation [18]. Yet the utilization of higher orders of the expansion parameter ε and determining the appropriate parameter expansion challenges the use of perturbation techniques for complex systems of coupled nonlinear equations [20]. In fact, many analytical investigations on the topic of multistable structural dynamics have given attention to bistable systems due to the relative simplicity of the theoretical formulations by virtue of the single degree-of-freedom (DOF). The narrower attention to bistable structures is also encouraged due to the wide range of applications from energy harvesting [21,22], to vibration control [23], to sensing [24]. The relative simplicity of the theoretical formulations for such single-DOF systems makes it possible to derive closed-from predictions of the strongly nonlinear responses of bistable oscillators [24].

Such straightforward analytical solution is often not possible for larger dimensional nonlinear systems [24]. As a result, a variety of methods have been employed to study multi-DOF nonlinear systems. Ritz methods utilizing quadratic polynomials of strain and deflection were shown by Mattioni et al. [25] to characterize the nonlinear deflections of multistable composite plates. Pirrera et al. [26] demonstrated that higher-order polynomials may be used to describe multi-event snap-through phenomena for such multistable composite structures. Describing function theory, propelled by Tanrikulu et al. [27], Chong and Imregun [28], Elizalde and Imregun [29], and Kalaycıoğlu and Özgüven [30], has delivered understanding on the steady-state, forced response that exacerbates the nonlinear resonant displacements of multi-DOF structures. While the formulations may require the system to exhibit symmetric nonlinearities [27] or may require an assumption of well-separated modes of vibration [28,31], a notable limitation of these methods is the assumption of input-output similarity. This prevents one from characterizing the co-existence of large amplitude snap-through dynamics and low amplitude oscillation around non-zero equilibria that may occur for multistable structures [11]. Alternatively, principles of equivalent linearization [32] have been used to characterize such near-to- and far-from-equilibrium responses of structures subjected to stochastic or harmonic excitations [33–35]. These methods rely on the formation and convergence of an equivalent linear stiffness matrix that enables the linearized equations to be solved via more conventional methods of analysis. To this end, Harne and Goodpaster [36] recently introduced an experimentally validated analytical formulation based on harmonic linearization [32] capable of predicting the steady-state dynamics of a built-up multistable structure. In contrast to methods based on describing function theory, both near-to- and far-from-equilibrium dynamic behaviors are able to be uncovered. The formulation [36] is also distinct from other equivalent linearization techniques by virtue of the implicit calculation of equivalent stiffness matrix terms in the process of obtaining the coupled, nonlinear algebraic equations to be solved for system response prediction. On the other hand, the nascent formulation lacks the means to shed insight on modal characteristics of multistable structures that may be contrasted to those of traditional linear dynamic systems. In addition, the extensibility of the formulation to characterize nonlinear systems represented by conventional ROM equations [13] has not been established. As a result, the knowledge on multistable structural dynamics manifest in myriad nonlinear systems, and their contrast to established linear systems, remains lacking.

This research aims to rectify these limitations via a comprehensive research undertaking. First, a new construct of the analysis [36] solution algorithms is fashioned, which becomes necessary to facilitate the new complement to conventional modal analysis [37]. Then, this unique modal formulation is leveraged to shed light on steady-state dynamics of multistable structures as they contrast with those modal behaviors of linear systems. Next, the analysis is significantly broadened to provision the study of multistable structures whose dynamic behaviors are governed by ROM-type equation systems. With these advancements, the clarity of the predictions is rigorously compared with those results obtained through the traditional time-stepping based simulations.

The remainder of this paper is organized as follows. In the next section, the preliminary analytical formulation is summarized. Then, the necessary advancements to the formulation established here are detailed. These improvements are then utilized to study qualitative characteristics of far-from-equilibrium dynamics in a modal perspective. The framework is then extended to accommodate nonlinearities and structural coupling manifest in ROM-based multistable structure models, and the efficacy and efficiency of the analytical predictions are characterized. A final section summarizes the achievements made and new understanding created through this research.

2. Analytical modeling: framework composition and new advancements

2.1. Example cases for analysis

In this research, two systems are examined in detail that exemplify the advancements made to the analysis of multistable structures subjected to harmonic loads. The two systems are shown schematically in Fig. 1. The first is analogous to the system studied in Ref. [36] and is shown in Fig. 1(a), which depicts three masses, coupled together via linear springs. Each mass has local viscous damping and nonlinear stiffness, which consists of negative linear and positive cubic stiffnesses. These local nonlinearities result in a multistable structural configuration with equilibria that are symmetric about $\mathbf{x}^* = \mathbf{0}$, and correspond to linearly coupled Duffing oscillators [38]. Each mass is subjected to an excitation force of the form $f_i = F_i \cos(\omega t + \phi_i)$, where the amplitude and phase of each excitation force may vary, but the frequency of the excitations is assumed to be the same across all DOF. The second system examined in this research is shown in Fig. 1(b). The system is a clamped-clamped beam similar to that studied via ROM simulation in Ref. [39]. The beam is subjected to a spatially uniform pressure distribution that harmonically varies in time by $p(t) = P_0 \cos(\omega t)$. The beam is perfectly flat when originally clamped before a thermal stress is introduced that leads the beam to buckle in a symmetric, bistable configuration.

2.2. Mathematical background of analytical framework

For completeness, a brief summary of the analytical framework by Harne and Goodpaster [36] is provided here. The formulation and algorithmic enhancements first undertaken in this research building upon this preliminary analytical framework empower the significant new knowledge gained through the subsequent sections via studies of modal characteristics and ROM-based compositions of multistable structures. To survey the preliminary framework [36], the general form of the governing equations of an n-DOF nonlinear dynamical system such as that shown in Fig. 1(a) is written in matrix form as (1).

$$\mathbf{M}\ddot{\mathbf{x}} + \mathbf{C}\dot{\mathbf{x}} + \mathbf{K}\mathbf{x} + \mathbf{N}(\mathbf{x}) = \mathbf{F} \tag{1}$$

The mass matrix, damping matrix, and linear stiffness matrix are given by (2).

$$\mathbf{M} = \mathrm{diag}[m_i]; \mathbf{C} = \mathrm{diag}[c_i]; \mathbf{K}_{ih} = \begin{cases} \sum_{h=1}^{n} k_{ih}; i = h \\ -k_{ih}; i \neq h \end{cases} \tag{2}$$

The generalized coordinates of each DOF and the corresponding generalized forces are denoted by (3).

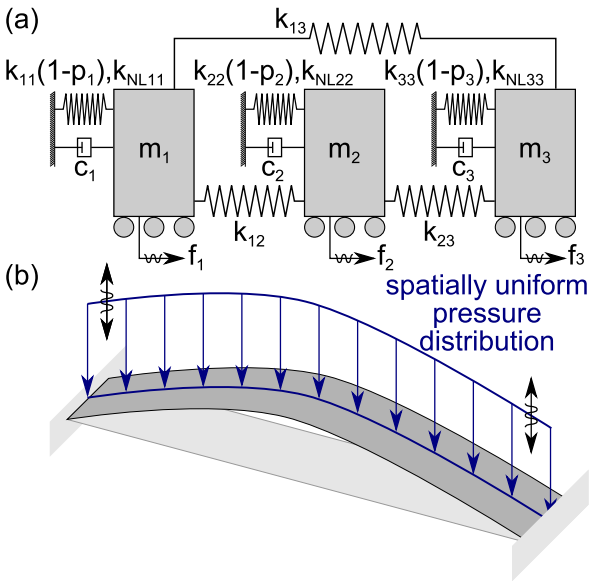

Fig. 1. Structural systems studied in this research. (a) Schematic of 3-DOF system with local nonlinearities, global linear coupling, and time-harmonic generalized excitation forces. (b) Schematic of clamped-clamped beam, thermomechanically stressed and subjected to a spatially uniform, time-harmonic pressure distribution.

$$\mathbf{x} = [x_1, x_2, \cdots, x_n]^T; \mathbf{F} = [f_1, f_2, \cdots, f_n]^T \tag{3}$$

The nonlinearities acting on the i^{th} DOF for the system considered in Fig. 1(a) are expressed in (4).

$$\mathbf{N}(\mathbf{x})_i = -k_{ii}p_i x_i + k_{NLii}x_i^3 \tag{4}$$

In (4), the negative stiffness that is introduced by the non-dimensional loading parameter p_i is treated as a form of nonlinearity. Clearly, the nonlinearities in this system are local to each generalized DOF, as seen by their inclusion in the grounded springs of Fig. 1(a). This is a simplification of the more general case where nonlinear coupling exists between all DOF that will be examined in Sec. 2.6 of this work. Yet, the assumption of local nonlinear stiffness influences utilized in this Sec. 2.2 provides a baseline for a model formulation [36] that delivers first insight on the steady-state dynamic behaviors of a representative multistable structure.

In general, the static equilibria of the system $\mathbf{x}^*$ are non-zero and are determined by solving (5).

$$\mathbf{K}\mathbf{x}^* + \mathbf{N}(\mathbf{x}^*) = \mathbf{0} \tag{5}$$

By applying a linearized Taylor's series expansion of (1) around a set of static equilibria $\mathbf{x}^*$, the linear response of the system is governed by (6).

$$\mathbf{M}\ddot{\mathbf{x}} + \mathbf{C}\dot{\mathbf{x}} + \{\mathbf{K} + \mathbf{K_L}\}\mathbf{x} = \mathbf{F} \tag{6}$$

In (6), the amendment to the linear stiffness matrix is derived to be (7).

$$\mathbf{K_L} = \mathrm{diag}\left[-k_{ii}p_i + 3k_{NLii}x_i^{*2}\right] \tag{7}$$

The linear, forced, steady-state response $\mathbf{x} = \mathbf{X}\mathbf{e}^{j\omega t}$ is then solved under the assumption of harmonic excitation $\mathbf{F} = \mathbf{f}\mathbf{e}^{j\omega t}$, where $j = \sqrt{-1}$. It is understood that the actual system response in time is the real component of $\mathbf{x}$. Note that in general, $\mathbf{f}$ and $\mathbf{X}$ may be complex such that the input forces and response dynamics, respectively, may oscillate out-of-phase.

The nonlinear forced response is found by utilizing procedures of stochastic or harmonic linearization [32]. This procedure yields an equivalent system in the form of (8).

$$\mathbf{M}\ddot{\mathbf{x}} + \mathbf{C}\dot{\mathbf{x}} + \{\mathbf{K} + \mathbf{K_e}\}\mathbf{x} = \mathbf{F} \tag{8}$$

The components of the equivalent linear stiffness matrix $(\mathbf{K_e})_{ih}$ are computed from (9).

$$(\mathbf{K_e})_{ih} = \frac{\langle g_{ih}w_{ih}\rangle}{\langle w_{ih}^2\rangle}; \mathbf{N}_i = \sum_{h=1}^{n} g_{ih}(w_{ih}); w_{ih} = \begin{cases} x_i - x_h & , i \neq h \\ x_i & , i = h \end{cases} \tag{9}$$

The $\langle\rangle$ brackets in (9) denote the mathematical expectation. Following Spanos and Iwan [40], the expectation for a deterministic system of equations subjected to harmonic excitation is defined as a time average over one period of the excitation. To calculate the entries of $\mathbf{K_e}$, one assumes the response to be of the form (10).

$$\mathbf{x} = \mathbf{q} + \mathbf{r}\mathbf{e}^{j\omega t} \tag{10}$$

where the biases $\mathbf{q}$ are real and the response amplitudes $\mathbf{r}$ are complex. For the nonlinearities given by (4), $\mathbf{K_e}$ is found to be (11).

$$\mathbf{K_e} = \mathrm{diag}\left(-k_{ii}p_i + k_{NLii}\left[3q_i^2 + \frac{3}{4}r_i^2\right]\right) \tag{11}$$

Note that $\mathbf{K_e}$ is diagonal because the nonlinearities are local to each DOF. Substituting the assumed solution (10) into the equivalent nonlinear governing Eq. (8), one obtains a system of equations to be simultaneously solved. After substituting (10) into (1), the Eq. (12) is obtained by the integration of Eq. (1) over a period $2\pi/\omega$ of the harmonic forcing. Eq. (13) is the equation of coefficients and parameters dependent upon a time-harmonic variation of $e^{j\omega t}$.

$$\left\{\mathbf{K} + \mathrm{diag}\left(-k_{ii}p_i + k_{NLii}\left[q_i^2 + \frac{3}{2}r_i^2\right]\right)\right\}\mathbf{q} = \mathbf{0} \tag{12}$$

$$\left\{ -\omega^2\mathbf{M} + \mathbf{j}\omega\mathbf{C} + \mathbf{K} \right\}\mathbf{r} + \mathbf{K_e}(\mathbf{q},\mathbf{r})\mathbf{r} = \mathbf{F} \tag{13}$$

Solving (12) and (13) yields the complex response amplitude and bias of the dynamic response of each generalized coordinate. While equivalent linear stiffness methods have been investigated previously in the context of nonlinear structural dynamics, the method utilized in this work, relying on an assumed harmonic solution (10), is unique with respect to previous approaches that derive the equivalent stiffness matrix via a series of proscribed static displacements [34]. This analysis calculates the equivalent linear stiffness matrix (11) implicitly during the solution procedure and facilitates both monostable and multistable structural dynamic response predictions for harmonic excitations. Utilizing this procedure, Harne and Goodpaster [36] have previously shown that analytical predictions of both near-to- and far-from- equilibrium dynamics agree qualitatively and quantitatively with numerical simulation and experimental measurements.

Yet, to greatly enhance the predictive capabilities of this analytical approach, a normalization scheme is required before the solution to Eqs. (12) and (13) should be attempted.

2.3. Normalization approach

The first technical undertaking in this research is to normalize (12) and (13). The normalization scheme is inspired by traditional modal analysis principles [37] that motivate a comparable new perspective on the equivalent modal responses of multistable structures. First, a coordinate transformation (14) is introduced.

$$\mathbf{z} = \mathbf{M}^{1/2}\mathbf{x} \tag{14}$$

Then, (14) is substituted into (1) and the equation system is pre-multiplied by $\mathbf{M}^{-1/2}$ to yield (15),

$$\ddot{\mathbf{z}} + \overline{\mathbf{C}}\dot{\mathbf{z}} + \overline{\mathbf{K}}\mathbf{z} + \overline{\mathbf{N}}(\mathbf{z}) = \overline{\mathbf{F}} \tag{15}$$

where $\overline{\mathbf{C}} = \mathbf{M}^{-1/2}\mathbf{C}\mathbf{M}^{-1/2}$, $\overline{\mathbf{K}} = \mathbf{M}^{-1/2}\mathbf{K}\mathbf{M}^{-1/2}$, $\overline{\mathbf{N}}(\mathbf{z}) = \mathbf{M}^{-1/2}\mathbf{N}(\mathbf{M}^{-1/2}\mathbf{z})$, and $\overline{\mathbf{F}} = \mathbf{M}^{-1/2}\mathbf{F}$. For a large class of problems in structural dynamics, $\overline{\mathbf{K}}$ is symmetric, thus enabling the solution to the eigenvalue problem for the undamped, linear system given by (16) [37].

$$\ddot{\mathbf{z}} + \left\{\overline{\mathbf{K}} + \overline{\mathbf{K}}_\mathbf{L}\right\}\mathbf{z} = \mathbf{0} \tag{16}$$

In (16), $\overline{\mathbf{K}}_\mathbf{L} = \mathbf{M}^{-1/2}\mathbf{K}_\mathbf{L}\mathbf{M}^{-1/2}$ is the mass-normalized amendment to the linear stiffness matrix (7). To normalize the length dimension of the system, a composite term is identified (17),

$$x_0 = x_c + x^*_{\max} \tag{17}$$

where x_c is a characteristic length such as a thickness or span of the structure, and $x^*_{\max}$ is the largest amplitude of a symmetric stable equilibria pair spanning $[-x^*_{\max}, x^*_{\max}]$ for the i^{th} generalized coordinate that exhibits this peak-to-peak range of statically stable configurations. The definition of a characteristic length employed in (17) is uniquely required for multistable structures since the possibility for non-zero entries of $\mathbf{x}^*$ encourages accounting for both system characteristics of the statically deformed configuration and system geometry in the normalization.

The fundamental eigenfrequency of (16) is defined to be λ_0 such that the fundamental natural frequency of the system is $\omega_0 = \sqrt{\lambda_0}$. For this definition of ω_0, the set of stable equilibria containing $x^*_{\max}$ from (17) is used when calculating $\overline{\mathbf{K}}_\mathbf{L}$ from (7). Once ω_0 is selected, a normalized time τ is introduced (18).

$$\tau = \omega_0 t \tag{18}$$

This normalized time τ also leads to the definition of a normalized excitation frequency (19).

$$\widehat{\omega} = \frac{\omega}{\omega_0} \tag{19}$$

This selection of the fundamental natural frequency ω_0 and normalized excitation frequency $\widehat{\omega}$ yields displacement responses with the lowest order resonance near $\widehat{\omega} = 1$.

The normalized, generalized coordinates of the system are given by (20).

$$\mathbf{y} = \frac{1}{x_0}\mathbf{z} \tag{20}$$

Substituting (18) and (20) into (15) yields the normalized governing equations of motion (21).

$$\mathbf{y}'' + \widehat{\mathbf{C}}\mathbf{y}' + \widehat{\mathbf{K}}\mathbf{y} + \widehat{\mathbf{N}}(\mathbf{y}) = \widehat{\mathbf{F}} \tag{21}$$

In (21), $()' = \frac{\mathbf{d}()}{\mathbf{d}\tau}$ and the normalized matrices and vectors of (21) are as follows.

$$\left(\widehat{\mathbf{C}}\right)_{ij} = \frac{1}{\omega_0}\frac{\psi}{\sqrt{m_{ii}m_{jj}}}; \psi = \begin{cases} \sum_{j=1}^{n} c_{ij} & , i = j \\ -c_{ij} & , i \neq j \end{cases} \tag{22}$$

$$\left(\widehat{\mathbf{K}}\right)_{ij} = \frac{1}{\omega_0^2}\frac{\varphi}{\sqrt{m_{ii}m_{jj}}}; \varphi = \begin{cases} \sum_{j=1}^{n} k_{ij} & , i = j \\ -k_{ij} & , i \neq j \end{cases} \tag{23}$$

$$\left(\widehat{\mathbf{N}}\right)_i = \frac{1}{\omega_0}\left(-\frac{k_{ii}p_i}{m_{ii}}y_i + \frac{x_0^2 k_{NLii}}{m_{ii}^2}y_i^3\right) \tag{24}$$

$$\left(\widehat{\mathbf{F}}\right)_i = \frac{f_i}{x_0\omega_0^2\sqrt{m_{ii}}} \tag{25}$$

The normalized system of Eq. (21) is then expressed as the equivalent linear system (26), following established harmonic or stochastic linearization techniques [32,41].

$$\mathbf{y}'' + \widehat{\mathbf{C}}\mathbf{y}' + \left\{\widehat{\mathbf{K}} + \widehat{\mathbf{K}}_\mathbf{e}\right\}\mathbf{y} = \widehat{\mathbf{F}} \tag{26}$$

The assumed response solution to the system of Eq. (26) is (27).

$$\mathbf{y} = \widehat{\mathbf{q}} + \widehat{\mathbf{r}}\mathbf{e}^{\mathbf{j}\widehat{\omega}t} \tag{27}$$

In (27), $\widehat{\mathbf{q}}$ and $\widehat{\mathbf{r}}$ denote the normalized response biases (real) and amplitudes (complex), respectively. Substituting the assumed solution (27) into (9), the elements of the normalized equivalent linear stiffness matrix $\widehat{\mathbf{K}}_\mathbf{e}$ are calculated to be (28).

$$\widehat{\mathbf{K}}_\mathbf{e} = \mathrm{diag}\left(-\frac{k_{ii}p_i}{\omega_0^2 m_{ii}} + \frac{x_0^2 k_{NLii}}{\omega_0^2 m_{ii}^2}\left[3\widehat{q}_i^2 + \frac{3}{4}\widehat{r}_i^2\right]\right) \tag{28}$$

The assumed solution (27) is then substituted into (21) and an integration is taken over one period of harmonic forcing. The result is (29), while (30) is the equation of coefficients dependent upon $e^{j\widehat{\omega}t}$ obtained by substituting (27) into (26).

$$\left\{\widehat{\mathbf{K}} + \mathrm{diag}\left(-\frac{k_{ii}p_i}{\omega_0^2 m_{ii}} + \frac{x_0^2 k_{NLii}}{\omega_0^2 m_{ii}^2}\left[\widehat{q}_i^2 + \frac{3}{2}\widehat{r}_i^2\right]\right)\right\}\widehat{\mathbf{q}} = \mathbf{0} \tag{29}$$

$$\left\{-\widehat{\omega}^2\mathbf{I} + j\widehat{\omega}\widehat{\mathbf{C}} + \widehat{\mathbf{K}}\right\}\widehat{\mathbf{r}} + \widehat{\mathbf{K}}_\mathbf{e}(\widehat{\mathbf{q}}, \widehat{\mathbf{r}})\widehat{\mathbf{r}} = \widehat{\mathbf{F}} \tag{30}$$

Together, (29) and (30) form a coupled set of nonlinear algebraic equations that are simultaneously solved to predict the forced, displacement response of the normalized structural system governed by (21).

2.4. Initial guess algorithm enhancements

In addition to normalization, the algorithm to select initial guesses for solutions is significantly enhanced in this research to obtain more complete analytical response predictions. The solution procedure employed in Ref. [36] requires the use of a conventional numerical algorithm to determine the response amplitudes $\mathbf{r}$ and biases $\mathbf{q}$ for a given set of system parameters and excitation conditions. The numerical solver utilized in Ref. [36] uses a nonlinear least squares cost function minimization technique to solve the system of equations. The seeding of accurate initial guesses is essential to the completeness and efficiency of the solution procedure because (i) seeding near the linear response may result in predictions for a small proportion

of the nonlinear dynamics, and (ii) seeding too far away from an actual solution may dramatically increase time required to converge via the algorithm. Thus, a strategic initial guess procedure is required to leverage the full capability of the analytical predictions.

In this research, the enhanced initial guess algorithm that is established is described as follows and depicted in the flowchart of Fig. 2. At each increment of an excitation parameter sweep, such as for the first frequency in an analytical 'frequency sweep', the derived algebraic equations are solved a number of times utilizing different initial guesses. For the first solution attempt in any sequence of solution-finding, the initial guess response amplitudes **r** are chosen to be perturbations away from the underlying linear response by a constant multiplier and small random value. The assumed biases **q** are set to be the corresponding static equilibria. In this way, an initial knowledge of the linearized system is strongly desirable to facilitate the efficient prediction of near-to-equilibrium dynamic responses, which may or may not be nonlinear. After the initial guess and solution procedure for the first parameter sweep increment and then the subsequent set of solution predictions, 25% of the initial guesses are the result of the previous parameter sweep increment as the initial condition for the current solution attempt. This proportion is allocated since it is likely that the solution to the algebraic equations using a small increment change will not be dramatically different than the previous iteration using a slightly different parameter increment. Such an approach inherently accounts for hysteretic effects observed for parameter changes associated with increasing or decreasing values. In other words, parameter sweeps utilizing both increasing and decreasing parameter values ensure the hysteresis is thoroughly characterized in regimes where coexisting behaviors are prevalent.

To aid in the prediction of snap-through responses, another 25% of initial guesses utilize generalized coordinate amplitudes **r** that are random perturbations away from one-half the span of a set of static equilibria, while the biases **q** are set to zero. The real and imaginary components of the response amplitude guesses are arbitrarily assigned to account for multiple snap-through states that may exhibit different phases of oscillation. This selection is based on the knowledge that snap-through occurs between static equilibria, so it is anticipated that the amplitude of the response will be close to one-half the peak distance between stable equilibria. For a system with symmetric sets of static equilibria, such as in Fig. 1(a), it is anticipated that the biases of snap-through responses will be zero due to the symmetry inherent to the interwell dynamics. Additionally, the magnitude of the predicted response amplitudes **r** are compared to the amplitude of the underlying linear response after each parameter sweep iteration to determine if any snap-through responses are calculated. If no snap-through dynamics are predicted for a set number of consecutive frequency increments, the analysis stops utilizing the snap-through initial guess seeding in order to increase the speed of the analytical response prediction. This check is depicted in the bottom half of Fig. 2, and is based on the a priori knowledge that snap-through of symmetric structural systems is a non-resonant

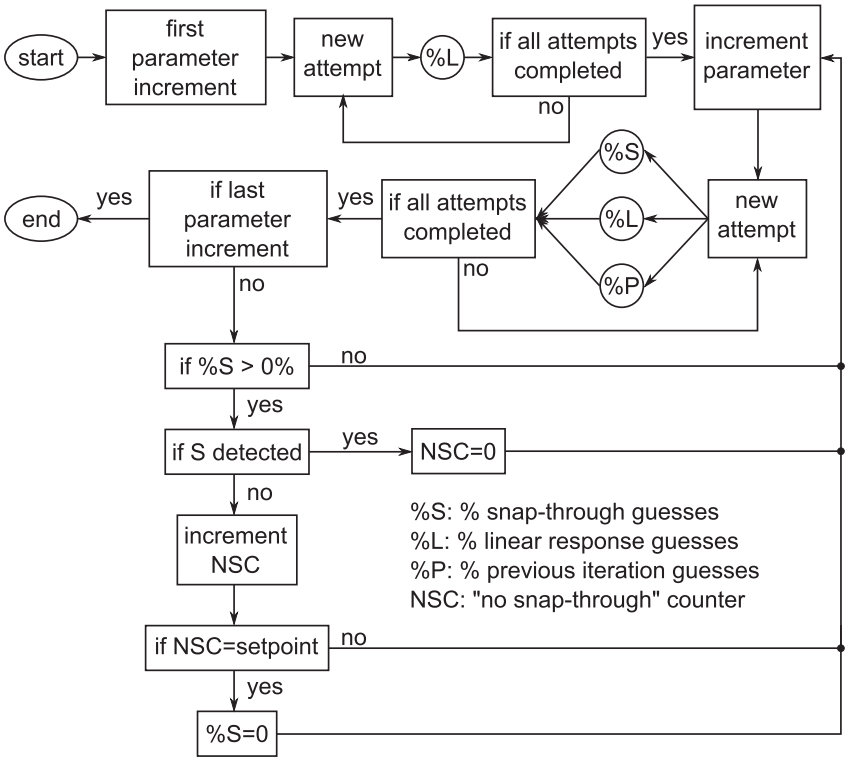

Fig. 2. Flowchart depicting enhanced algorithm used to seed initial guesses when solving the nonlinear algebraic equations derived by analysis to robustly predict all coexistent dynamic responses.

phenomenon that originates at low frequencies. The remaining initial guesses – either 50% or 75% of the total employed, depending on whether the algorithm is looking for snap-through responses – are chosen as random perturbations away from the underlying linear response.

The algorithm articulated in this Sec. 2.4 is designed to facilitate efficient predictions for parameter sweeps of symmetric structural systems. Alterations to the algorithm may be made to further enhance the versatility of the approach. For example, if the nonlinear dynamic responses are sought for only a single set of forcing parameters, the solution procedure should utilize both linear and snap-through initial guess conditions in order to identify all potential near-to- and far-from-equilibrium dynamics. The algorithm can also be enhanced for structures that are expected to exhibit interwell oscillations for parameter values that are not at extremes of the parameter range, such as asymmetric Duffing oscillators [42]. This may be accomplished by periodically utilizing snap-through initial guesses at every n^{th} parameter increment, where n is a set integer. When snap-through dynamics are predicted for the first time, snap-through initial guesses should then be utilized at every parameter increment until the cut-off frequency criteria are met. Performing such a sweep with both increasing and decreasing parameter values would ensure complete analytical dynamic predictions.

2.5. Equivalent nonlinear modal response

In addition to dynamic response predictions, the system described by (1) is scrutinized in this research from a modal perspective relevant for multistable structures. The equivalent linear stiffness matrix (11) contributes to the equivalent linear system response via (8). Thus, conventional modal analysis procedures [37] may be utilized to illuminate a new modal interpretation of the multistable dynamic system behavior, thus permitting comparison to other linear and nonlinear modal interpretations [43].

To this end, an equivalent modal coordinate is introduced using (31).

$$\mathbf{v} = \tilde{\mathbf{P}}^{-1}\mathbf{M}^{-1/2}\mathbf{x} \tag{31}$$

The matrix of equivalent eigenvectors $\tilde{\mathbf{P}}$ is computed from the matrix (32).

$$\tilde{\mathbf{K}} = \mathbf{M}^{-1/2}\{\mathbf{K} + \mathbf{K_e}\}\mathbf{M}^{-1/2} \tag{32}$$

The corresponding eigenvalues of $\tilde{\mathbf{K}}$ are collected in a diagonal matrix $\tilde{\mathbf{\Lambda}}$. Substitution of (31) into (8) leads to (33).

$$\ddot{\mathbf{v}} + \tilde{\mathbf{\Theta}}\dot{\mathbf{v}} + \tilde{\mathbf{\Lambda}}\mathbf{v} = \tilde{\mathbf{F}} \tag{33}$$

where

$$\tilde{\mathbf{\Theta}} = \mathrm{diag}(2\zeta_i\omega_i) \tag{34}$$

$$\tilde{\mathbf{\Lambda}} = \mathrm{diag}\left(\omega_i^2\right) \tag{35}$$

$$\tilde{\mathbf{F}} = \mathbf{P}^T\mathbf{M}^{-1/2}\mathbf{F} \tag{36}$$

In (34)–(36), ζ_i and ω_i are the damping ratio and angular natural frequency, respectively, of the i^{th} equivalent mode. The study of the eigenvectors $\tilde{\mathbf{P}}$, eigenvalues $\tilde{\mathbf{\Lambda}}$, and equivalent nonlinear modal coordinates $\mathbf{v}$ aids in understanding the underlying dynamic response of multistable structures. Consequently, this research investigates the characteristics of the equivalent nonlinear modal responses and their corresponding eigenvectors to uncover unique insight into the dynamics of multistable structures. The completeness of the analytical response predictions is necessary to capitalize on the assessment of such newly formulated equivalent nonlinear modes. Indeed, the complete analytical predictions are facilitated by the normalization scheme of Sec. 2.3 and the algorithmic enhancements articulated in Sec. 2.4.

2.6. Generalization of the analytical framework to global nonlinearities

While the local nonlinearities expressed by (4) have practical justifications [44,45], it has been shown that aerostructural systems can be modeled using reduced order models (ROMs) that account for coupling among DOFs according to products of generalized coordinate responses [13,46]. In Ref. [39], such a ROM was formulated for a thermomechanically loaded beam that may be warped into a post-buckled state via thermal stresses. This induces multistability for the various modes of vibration caused by harmonic forced response. In this ROM, the equation of motion for the i^{th} generalized coordinate is (37) [39].

$$(\mathbf{M})_{ij}\ddot{y}_j + (\mathbf{C})_{ij}\dot{y}_j + (\mathbf{K})_{ij}y_j - \Delta T\left(\mathbf{K}^{(\mathbf{1})}\right)_{ij}y_j + \left(\mathbf{K}^{(\mathbf{2})}\right)_{ijk}y_j y_k + \left(\mathbf{K}^{(\mathbf{3})}\right)_{ijkl}y_j y_k y_l = f_i \tag{37}$$

In (37), the repeated subscript index indicates a repeated summation over all n DOF. The determination of ROMs in the form of (37) requires the identification of the linear and nonlinear stiffnesses that are induced by the elastic and thermal stresses acting on the system. The coefficients $(\mathbf{K}^{(\mathbf{1})})_{ij}$ are associated with linear stiffnesses resulting from the mean thermal load, expressed as a temperature difference ΔT with respect to a reference temperature. The temperature difference ΔT in (37) acts in an analogous way to the load parameter p in (7) because for increasing positive values of ΔT the matrix entries $(\mathbf{K}^{(1)})_{ij}$, which are primarily positive, may cause a net negative linear stiffness when combined with the counterpart terms of $(\mathbf{K})_{ij}$. The $(\mathbf{K}^{(\mathbf{2})})_{ijk}$ and $(\mathbf{K}^{(3)})_{ijkl}$ are quadratic and cubic stiffness coefficients, respectively, and are associated with thermal and elastic stresses.

Clearly, the nonlinearities in (37) represent a more complete and complex nonlinear interaction among the n generalized coordinates than the local nonlinear forces acting in (1). Therefore, a more general approach to the linearization method of the analytical framework must be employed. In particular, (9), used previously to derive the effective stiffness matrix $\mathbf{K_e}$, is primarily valid if the DOF are coupled in chain-like configurations, similar to the system schematic shown in Fig. 1(a). Yet, for the ROM system (37), global nonlinear coupling among the generalized coordinates via products of the responses prevents the adoption of (9). A general outcome of stochastic linearization [32] demonstrates that the equivalent linear stiffness matrix entries $(\mathbf{K_e})_{ih}$ relating the i^{th} and h^{th} generalized coordinates are given by (38).

$$(\mathbf{K_e})_{ih} = \langle\frac{\partial N_i}{\partial x_h}\rangle \tag{38}$$

In (38), N_i is the nonlinearity acting on the i^{th} DOF. Applying (38) to the governing equations of the ROM (37) yields the linearized Eq. (39).

$$\mathbf{M}\ddot{\mathbf{y}} + \mathbf{C}\dot{\mathbf{y}} + \left\{\mathbf{K} - \mathbf{K_e^{(1)}} + \mathbf{K_e^{(2)}} + \mathbf{K_e^{(3)}}\right\}\mathbf{y} = \mathbf{F} \tag{39}$$

In (39), the components of the equivalent linear, quadratic, and cubic stiffness matrices are given by (40).

$$\left(\mathbf{K_e^{(1)}}\right)_{ih} = \langle\frac{\partial\left(\Delta T(\mathbf{K^{(1)}})_{ih}y_j\right)}{\partial y_h}\rangle;\ \left(\mathbf{K_e^{(2)}}\right)_{ih} = \langle\frac{\partial\left((\mathbf{K^{(2)}})_{ijk}y_j y_k\right)}{\partial y_h}\rangle;\ \left(\mathbf{K_e^{(3)}}\right)_{ih} = \langle\frac{\partial\left((\mathbf{K^{(3)}})_{ijkl}y_j y_k y_l\right)}{\partial y_h}\rangle \tag{40}$$

To calculate the entries of (40), an assumed solution of the form of (41) is introduced as before.

$$\mathbf{y} = \mathbf{q} + \mathbf{re}^{\mathbf{j}\omega t} \tag{41}$$

Applying (41) to (40), the entries of the equivalent stiffness matrices are as follows.

$$\left(\mathbf{K_e^{(1)}}\right)_{ij} = \Delta T\left(\mathbf{K^{(1)}}\right)_{ik}\delta_{jk} \tag{42}$$

$$\left(\mathbf{K_e^{(2)}}\right)_{ij} = \left\{\left(\mathbf{K^{(2)}}\right)_{ijk} + \left(\mathbf{K^{(2)}}\right)_{ikj}\right\}q_k \tag{43}$$

$$\left(\mathbf{K_e^{(3)}}\right)_{ij} = \left\{\left(\mathbf{K^{(3)}}\right)_{ijkl} + \left(\mathbf{K^{(3)}}\right)_{ijlk} + \left(\mathbf{K^{(3)}}\right)_{iljk}\right\}q_k q_l + \frac{1}{4}\left\{\left(\mathbf{K^{(3)}}\right)_{ijkl} + \left(\mathbf{K^{(3)}}\right)_{ijlk} + \left(\mathbf{K^{(3)}}\right)_{iljk}\right\}r_k r_l \tag{44}$$

In (42), δ_{jk} is the Kronecker delta function. After the substitution of (41) into (37), the Eq. (45) is then obtained by integrating (37) over one period of the harmonic excitation force. The Eq. (46) is the coefficient of parameters dependent upon $e^{j\omega t}$ after substituting the assumed solution (41) into the equivalent governing Eq. (39).

$$\left\{\mathbf{K} - \Delta T\mathbf{K}^{(1)}\right\}\mathbf{q} + \boldsymbol{\kappa}^{(2)} + \boldsymbol{\kappa}^{(3)} = \mathbf{0} \tag{45}$$

$$\left\{-\omega^2\mathbf{M} + \mathbf{j}\omega\mathbf{C} + \mathbf{K}\right\}\mathbf{r} + \left[-\mathbf{K_e^{(1)}} + \mathbf{K_e^{(2)}} + \mathbf{K_e^{(3)}}\right]\mathbf{r} = \mathbf{F} \tag{46}$$

In (45), the i^{th} component of the vectors $\boldsymbol{\kappa}^{(\mathbf{2})}$ and $\boldsymbol{\kappa}^{(\mathbf{3})}$ are given by (47) and (48), respectively.

$$\left(\kappa^{(\mathbf{2})}\right)_i = \left(\mathbf{K}^{(\mathbf{2})}\right)_{ijk} q_j q_k + \frac{1}{2}\left(\mathbf{K}^{(\mathbf{2})}\right)_{ijk} r_j r_k \tag{47}$$

$$\left(\kappa^{(\mathbf{3})}\right)_i = \left(\mathbf{K}^{(\mathbf{3})}\right)_{ijkl} q_j q_k q_l + \frac{1}{2}\left(\left(\mathbf{K}^{(\mathbf{3})}\right)_{ijkl} + \left(\mathbf{K}^{(\mathbf{3})}\right)_{ijlk} + \left(\mathbf{K}^{(\mathbf{3})}\right)_{iljk}\right) q_j r_k r_l \tag{48}$$

Solving (45) and (46) simultaneously results in the offsets $\mathbf{q}$ and complex response amplitudes $\mathbf{r}$. Once these response predictions are made for the system in (37), the physical displacement $w(x,t)$ is reconstructed from the n generalized coordinates $\mathbf{y}(t)$ (41) and basis functions $\psi(x)$ via (49).

$$w(x,t) = \sum_{i=1}^{n} y_i(t)\psi_i(x) \tag{49}$$

3. Local nonlinearities and global linear coupling

Building from the previous analytical framework [36] described in Sec 2.2, this research establishes comprehensive and significant advancements to the method via the normalization (Sec. 2.3), strategic initial guess procedure (Sec. 2.4), equivalent modal examination approach (Sec. 2.5), and extension to a broader class of nonlinearities manifest in myriad ROMs (Sec. 2.6). In this Sec. 3, the aim is to assess the success of these new technical contributions to the analytical framework in the context of the lumped-parameter multistable system schematically shown in Fig. 1(a). Sec. 4 examines comparable aspects pertaining to general ROMs, like the model of the post-buckled beam shown in Fig. 1(b).

3.1. Assessment of analytical framework advancements

The efficacy and completeness of the enhanced analytical framework and strategic initial guess procedure are first assessed with attention to the system shown schematically in Fig. 1(a) having local nonlinearities and global linear coupling. A set of structural and excitation parameters are chosen to represent a lightly damped multistable structural system, similar to the experimental beam structure examined in Ref. [36]. These parameters are provided in the Appendix. Fig. 3 compares the generalized displacement amplitudes $|\mathbf{r}|$ of the analytical predictions using the original dimensioned formulation Fig. 3(a–c), and using the normalized formulation Fig. 3(d–f). At each frequency parameter, the nonlinear algebraic Eqs. (29) and (30) are solved with 96 different sets of initial guesses, chosen via the algorithm discussed in Sec. 2.4. The results generated by employing the normalized analysis are reconstructed back to the generalized coordinates via (14) and (19). In Fig. 3, the simulation results used to verify the efficacy of the analytical procedure of Sec. 2 are obtained through a fourth-order Runge-Kutta numerical integration of the governing Eq. (1), and are shown by the dot data points in Fig. 3. This simulation technique is employed since it is efficient and stable for a large variety of nonlinear equation systems [47] and is widely utilized in

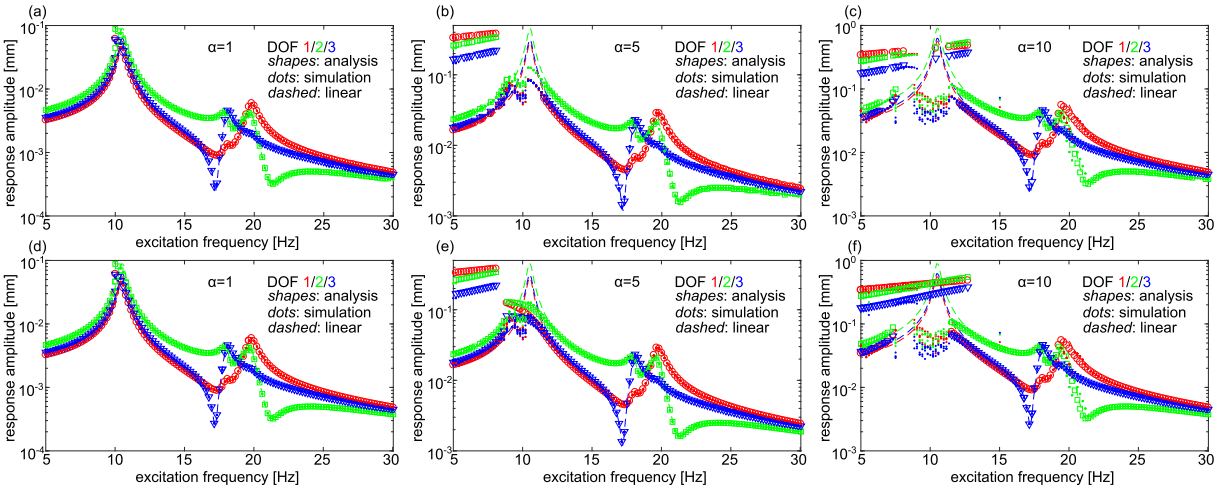

Fig. 3. Frequency response amplitudes of a representative structural configuration with local nonlinearities. (a–c) Results of simulation and dimensioned analysis for increasing excitation amplitudes. (d–f) Results of simulation and normalized analysis for increasing excitation amplitudes.

numerical computations of structural systems [48,49]. At each excitation frequency, the numerical integration is undertaken with 52 sets of displacement and velocity initial conditions that are randomly generated. With the aim to ensure that the simulation yields steady-state dynamic responses comparable to the analysis, the governing Eq. (1) are numerically integrated over 250 excitation periods and a fast Fourier transform (FFT) is taken over the last 50 excitation periods to produce the simulation data points in Fig. 3. To ensure accuracy of the simulations, 1024 time steps per excitation period are utilized in the numerical integration.

The columns of Fig. 3 show the evolution of the generalized displacement amplitudes with respect to increasing force amplitudes. Here, α denotes a scaling factor that is uniformly applied to the amplitudes of the excitation forces acting on each DOF. For $\alpha = 1$, the analysis agrees well with simulation regardless of the use of the normalization as shown in Fig. 3(a). The slight softening effect of a lowering of the first resonant peak at 10.5 Hz in Fig. 3(a, d) is reconstructed by all methods of solving the governing Eq. (1). For greater harmonic excitation force amplitudes via scaling parameter $\alpha = 5$, as shown in Fig. 3(b) and (e), the completeness of the dimensioned analytical predictions diminishes. Such degradation is seen in Fig. 3(b) where coexistent low amplitude intrawell and large amplitude snap-through dynamics, around 5–8 Hz and at 5 Hz, respectively, are predicted and identified by simulation. Yet, the dimensioned analysis fails to predict responses near the fundamental resonance near 10 Hz in Fig. 3(b).

By contrast, the normalized analysis seen in Fig. 3(e) more completely uncovers the snap-through displacement behaviors around 5–8 Hz in Fig. 3(e) and the trends of the softening intrawell oscillation amplitudes around 10 Hz. In fact, Fig. 3(e) exemplifies the utility of this analytical technique over other methods of multi-DOF nonlinear dynamical analysis. While the nonlinear broadening of the resonant frequency exhibited around 10 Hz is comparable to the nonlinear trends studied in detail via describing function theory, e.g. Ref. [27–30], the high-amplitude snap-through dynamics predicted in Fig. 3(e) have no such analogue. Considering these trends, the numerical results only predict snap-through dynamics around 5 Hz in Fig. 3(b,e), while both dimensioned and normalized analyses forecast interwell responses in the frequency bandwidth of 5–8 Hz. The discrepancy may be due to the single-harmonic assumption of the analysis, and provides evidence that the analytical formulations described in Sec. 2.2 and 2.3 yield conservative estimates of the displacement amplitude and frequency bandwidth of snap-through dynamics regimes.

Considering a still higher amplitude of the excitation forces $\alpha = 10$, Fig. 3(c) reveals that the dimensioned analysis fails to predict a large proportion of the snap-through responses near 5–12 Hz that are otherwise uncovered by the normalized analytical formulation solution, Fig. 3(f). Although the simulation results do not likewise identify as broad of a bandwidth of the large amplitude snap-through displacements, the analysis of bistable and multistable structures is known to provide conservative estimates [24,45] on thresholds of excitation conditions that may induce large amplitudes of displacement should perturbations act on the system. Overall, from the exemplary comparison of results in Fig. 3, it is evident that predictions of the generalized displacements by the original analysis are inferior in completeness when compared to the normalized analytical formulation. These enhancements are also further promoted by the strategic initial guess procedure that more effectively selects the initial vectors of $\mathbf{q}$ and $\mathbf{r}$ used in the least squares minimization of the nonlinear algebraic Eqs. (29) and (30). While the effects of the enhancements are not independently investigated, several conclusions may be inferred from these results.

Regardless of the normalization and initial guess enhancements, the analytical framework more rapidly generates predictions of the generalized coordinate forced response when compared to the direct simulation approach. The times required for the normalized analyses of Fig. 3(d–f) are 3.48, 3.67, and 2.77 ms per attempt to calculate a solution, respectively, compared to 826, 701, and 659 ms per attempt for the simulation results of Fig. 3(d–f). Thus, the normalized analytical results are 237, 191, and 238 times faster than the comparative simulation baselines. The reported times have units of ms per attempt, which accounts for the difference between the number of solution attempts used in the analysis and simulation results of Fig. 3. A portion of the decreased computational time can be attributed to the single-harmonic and steady-state assumptions used in the analysis of Sec. 2.3. Comparatively, the numerical integration of the governing equations captures all harmonics in the response, including chaotic regimes. The inclusion of each additional harmonic to be considered would result in an additional N nonlinear algebraic equations that couple with Eqs. (29) and (30), where N is the number of DOF. While the inclusion of other-order harmonics may increase computational times, an advantage may be that the inclusion of additional harmonics, such as the order 1/2 subharmonic, may illuminate additional bifurcation behaviors such as the period-doubling bifurcation that precedes chaos [50].

In addition to an enhanced ability to obtain accurate solutions from the derived algebraic equations utilizing similar attempts and numerical convergence criteria, the normalized analysis produces results approximately twice as fast as the dimensioned analysis and two orders of magnitude faster than simulation. All together, these results illustrate the efficacy of the new analytical framework improvements to deliver accurate predictions of highly nonlinear, far-from-equilibrium responses. The complete response predictions of the normalized framework will be harnessed in Sec. 3.2 for sake of illuminating the new modal formulation of multistable structural dynamics.

The analytical predictions calculate a complex response amplitude r_i and offset q_i for the i^{th} generalized coordinate, so that a time series of the analytical result may be reconstructed. Fig. 4 shows the contrast between the reconstructed analytical time series of generalized displacements as solid curves and the simulated results as dash-dot curves when the excitation frequency is 7.5 Hz and excitation amplitude scaling factor is $\alpha = 5$. The time series responses shown in Fig. 4(a) are the intrawell dynamics that coexist with the snap-through dynamics, which are shown in Fig. 4(b) for the same excitation

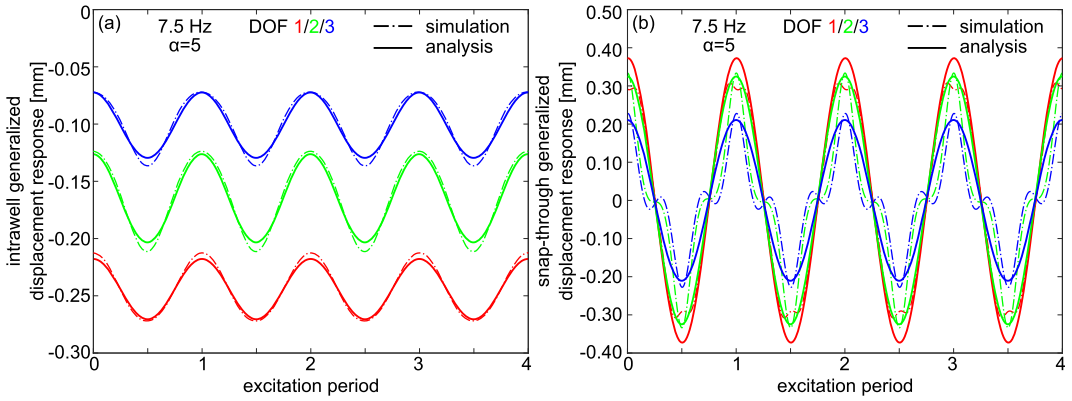

Fig. 4. Analytical and numerical time series at 7.5 Hz for $\alpha = 5$. (a) Intrawell dynamic responses. (b) Snap-through dynamic responses.

conditions. The analytical and simulated results are in good agreement. The errors between the analytical and simulated values of the RMS displacements for the intrawell oscillations in Fig. 4(a) are 0.20%, 0.060%, and 0.097%, respectively, for the first, second, and third generalized coordinates. The snap-through dynamics in Fig. 4(b) reconstructed by the analysis exhibit greater RMS error respecting the simulations. The RMS errors are 15%, 33%, and 30%, respectively, for the generalized coordinates. The errors grow for the case of snap-through oscillations due to the presence of higher-order harmonics. On the other hand, the errors in the peak-to-peak amplitudes of generalized displacement are much less: 21%, 2.7%, and 7.5%. Due to the higher-order harmonics captured through simulation, the largest RMS and peak-to-peak amplitude errors do not occur for the same DOF. From the perspective of the structural dynamics of air vehicles operating in extreme environments, a primary danger associated with the onset of snap-through oscillations for a multistable structure is fatigue damage [51], which is characterized by the difference between maximum and minimum stresses [52]. Thus, the peak-to-peak amplitude error may be more important than RMS error when contrasting the numerical simulation to the analytical approximation. In this light, the greater accuracy of the analytical peak-to-peak amplitude predictions when compared to the exact simulation results may be helpful to informing design and deployment decisions in the context of sonic fatigue of aerostructural systems.

3.2. Equivalent nonlinear modes

The normalized and enhanced analytical formulation facilitates the investigation of the concept of equivalent nonlinear modes (ENMs) established in Sec. 2.5. The analytical predictions used for the following ENM reconstruction are obtained from the three cases examined in Fig. 3(d–f). The frequency response of the ENM generalized coordinates $\mathbf{v}$ are displayed in Fig. 5(a) when the excitation amplitude scaling factor is $\alpha = 1$. The corresponding mode shapes of this system may be investigated by examining the eigenvectors of $\tilde{\mathbf{K}}$ from (26) on the surface of the unit sphere in $\mathbb{R}^3$ due to their normalized unit amplitudes. These mode shapes induced for $\alpha = 1$ are shown as a parametric plot in Fig. 5(b) where the changing parameter is

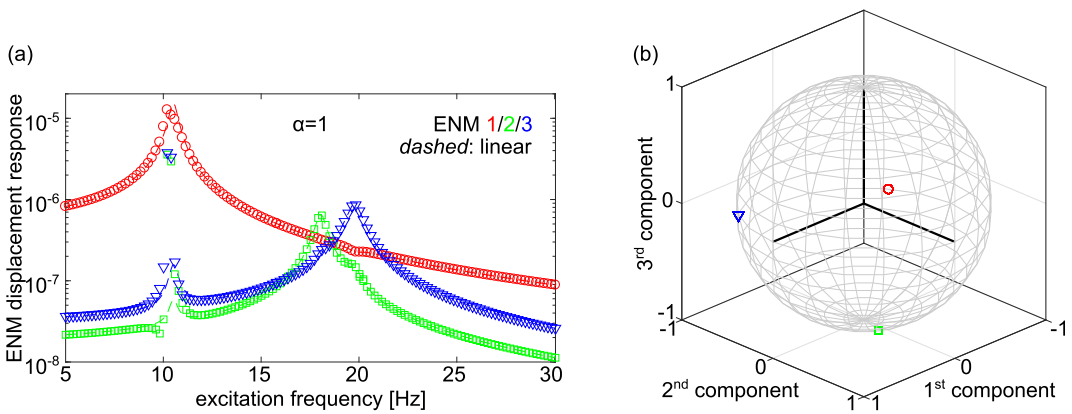

Fig. 5. Analytical results. (a) ENMs corresponding to $\alpha = 1$. (b) Characteristic eigenvectors corresponding to orthogonal mode shapes. The eigenvector corresponding to the first (second/third) eigenfrequency is red (green/blue). (For interpretation of the references to colour in this figure legend, the reader is referred to the Web version of this article.)

the excitation frequency. The eigenvector corresponding to the first (second, third) eigenfrequency of $\tilde{\mathbf{K}}$ is denoted by red circles (green squares, blue triangles).

One feature of ENMs that distinguishes them from linear modes is that, even for quasi-linear responses, the modal coordinates are coupled, such that each mode is more responsive at all resonant frequencies of system [43], which violates the assumption of well-separated modes in Refs. [28,31]. In Fig. 5(a), this is evident by the response amplitudes of ENMs 2 and 3, denoted by green and blue, respectively, that rise considerably to contribute near the first resonance frequency 10.5 Hz. The ENM amplitudes of modes 2 and 3 specifically increase by nearly two orders of magnitude very close to the resonant frequency, emphasizing the coupled nature of ENMs that is distinct from linear normal modes. Yet, the eigenvectors of $\tilde{\mathbf{K}}$ displayed in Fig. 5(b) remain essentially fixed revealing that for such low excitation amplitudes, the mode shapes of a multistable structure are independent of the frequency at which the structure is excited.

The frequency response of the ENMs are displayed in Fig. 6(a) for the case of increased excitation amplitude scaling factor to $\alpha = 5$, whose reconstructed generalized displacements are shown in Fig. 3(e). The lowest order ENM in Fig. 6(a) exhibits nonlinear resonant softening around 10.5 Hz to a more severe extent than the case with $\alpha = 1$. Likewise, the higher-order ENMs increase in contribution by over an order of magnitude to the collective nonlinear modal response near the lowest order resonant frequency. Thus, it is observed that all three ENMs contribute to the nonlinear intrawell dynamics near the fundamental linear resonance. The nonlinear softening trends exhibited are tracked by dark gray lines with filled circle terminations. The eigenvector translations of such nonlinear softening are manifest by deviations from the underlying linear mode shapes. Fig. 6(b) maps this frequency dependent deviation for the ENM eigenvectors associated with the dark gray lines with circular terminations.

At this higher excitation amplitude with scaling factor $\alpha = 5$, snap-through dynamics are observed from 5 to 8 Hz in the physical domain, Fig. 3(e), resulting in corresponding snap-through responses in the modal domain, denoted in Fig. 6(a) by light gray arrows. Unlike in the physical domain, in which the snap-through dynamics for each DOF are on the same order of magnitude of displacement, the snap-through responses of ENMs 2 and 3 are approximately two orders of magnitude less in amplitude than ENM 1. This closely correlates snap-through dynamics with a "lowest order" response associated with the first ENM. In contrast to nonlinear intrawell dynamics that exhibit large contributions from all three ENMs, high-amplitude interwell regimes are observed to primarily oscillate in the fundamental ENM. This explains why the higher-order ENMs have larger displacement amplitudes during the nonlinear intrawell dynamic than during snap-through. In fact, considering Fig. 6(a), the overall trends of the first ENM frequency response are analogous to the frequency response of a single-DOF, bistable Duffing oscillator [24]. This is a compelling result, because it reveals for the first time that the characteristic bistable Duffing oscillator frequency response is still preserved in multistable structures albeit via the fundamental equivalent normal mode. The snap-through responses of the ENMs are also uniquely identified by the eigenvectors of $\tilde{\mathbf{K}}$, denoted by light gray arrows in Fig. 6(b). Looking closely in Fig. 6(c–e), the snap-through eigenvectors are seen to be highly frequency-dependent by way of changing ENM contributions with each change in the excitation frequency, observed by the light gray arrow indicators.

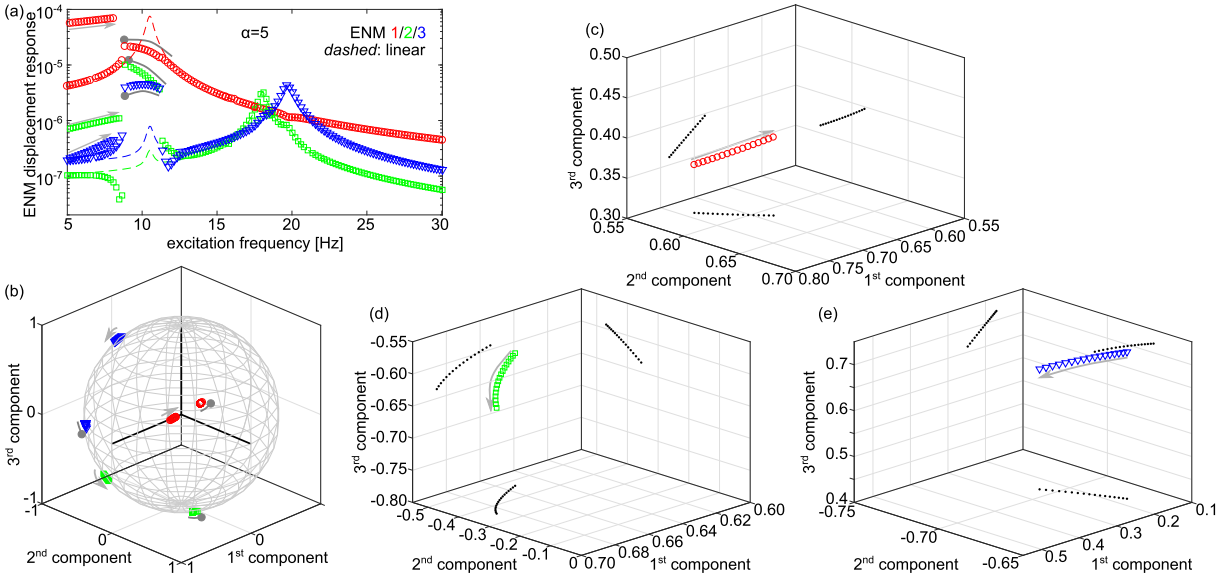

Fig. 6. Analytical results. (a) ENMs corresponding to $\alpha = 5$. (b) Characteristic eigenvectors corresponding to orthogonal mode shapes. The eigenvector corresponding to the first (second/third) eigenfrequency is red (green/blue). Intrawell nonlinear dynamics denoted by dark gray indicators. Progression of snap-through indicated by light gray arrows. (c–e) Frequency dependence of 1st/2nd/3rd snap-through eigenvectors, respectively. (For interpretation of the references to colour in this figure legend, the reader is referred to the Web version of this article.)

The trends observed in Fig. 6 with the presence of coexisting intrawell and snap-through oscillations are exacerbated when the excitation amplitude scaling factor is further increased to $\alpha = 10$. At this high excitation amplitude, the analysis no longer predicts intrawell dynamics near the first resonant peak at 10.5 Hz, and the more predominant, low frequency snap-through dynamics persist across a much broader frequency bandwidth. As a result, the intrawell ENM eigenvectors are mostly independent of excitation frequency, Fig. 7(b). On the other hand, the severely nonlinear snap-through responses exhibit pronounced frequency dependence in the eigenvector space Fig. 7(b). The light gray arrows in Fig. 7(b) relate the frequency dependence of the snap-through ENM eigenvectors that is more clearly evident in Fig. 7(c–e).

By adopting a new equivalent normal mode lens to scrutinize the dynamic response of multistable structures, the examinations of this section reveal several underlying aspects of multistability. The snap-through dynamics of the physical domain response lead to a lowest order ENM associated strictly with the large-amplitude snap-through response and small contribution from higher order ENMs. The eigenvectors of $\tilde{\mathbf{K}}$ corresponding to such snap-through behaviors exhibit strong frequency dependence and are inherently "far from" the eigenvectors associated with the intrawell ENMs. The latter intrawell eigenvectors, in turn, are closely aligned with the mode shapes of the underlying linear response by way of a mostly frequency independent property. In addition, the lowest order ENM of the multistable structure has a qualitative parallel to a single-DOF bistable Duffing oscillator, which suggests an intrinsic connection between high- and low-dimensional multistable structures with the single-DOF building block of a bistable structure [24]. These are new insights illuminated by the normalized and enhanced analytical formulation established in this research.

4. Global nonlinearities for ROM modal equations

The analytical method established previously [36] is amenable to investigate structural systems containing nonlinearities local to each DOF. In Sec. 3, it is shown that the normalization scheme (Sec. 2.3) and enhanced solution algorithm (Sec. 2.4) produce complete sets of analytical predictions two orders of magnitude faster than numerical integration of the governing Eq. (1), while a modal interpretation of the equivalent structural system (8) provides unique insights into high-dimensional multistable structural dynamics (Sec. 2.5). An additional aim of this research is to formulate a new modeling framework that encompasses global nonlinearities typically encountered in reduced order models (ROMs) of multi-physics structural systems. Using the analytical framework extension described in Sec 2.6, this Sec. 4 examines the fidelity of analytical predictions for the clamped-clamped beam shown in Fig. 1(b) whose nonlinear system model is formulated by a 4-mode ROM.

4.1. Mode shapes of clamped-clamped beam

The four, lowest order identified mode shapes of the clamped-clamped, thermomechanically loaded beam depicted in Fig. 1(b) are shown in Fig. 8. These modes are used to fashion a 4-mode ROM created via the implicit condensation method described in Ref. [53]. This ROM is used in this research to examine the capability for the newly developed analytical

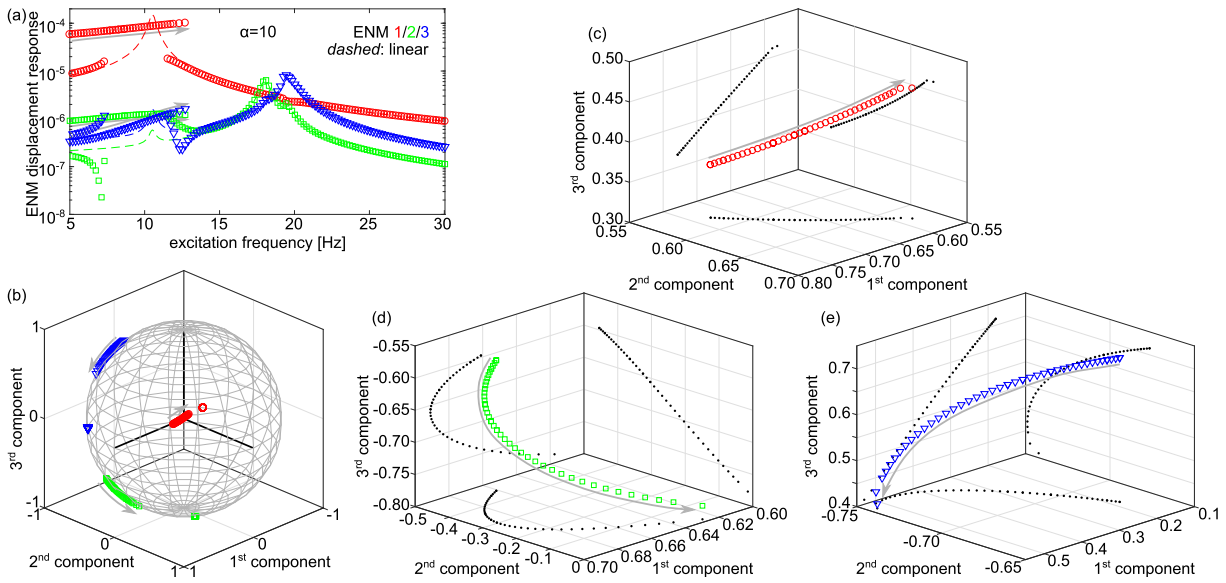

Fig. 7. Analytical results. (a) ENMs corresponding to $\alpha = 10$. (b) Characteristic eigenvectors corresponding to orthogonal mode shapes. The eigenvector corresponding to the first (second/third) eigenfrequency is red (green/blue). Progression of snap-through indicated by light gray arrows. (c–e) Frequency dependence of 1st/2nd/3rd snap-through eigenvectors, respectively. (For interpretation of the references to colour in this figure legend, the reader is referred to the Web version of this article.)

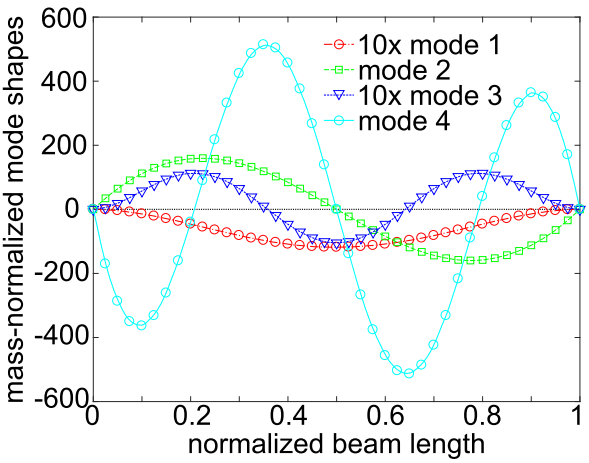

Fig. 8. First four mode shapes of clamped-clamped beam, modeled using a ROM-based system of equations.

framework of Sec. 2.6 to accurately predict the nonlinear response of a multistable structure governed by a ROM-based system of equations, thus greatly broadening the applicability of the analytical formulation as originally fashioned in Ref. [36]. The ROM-based system examined here marks a departure from previous analytical studies of multi-DOF nonlinear structures, which typically investigate systems with a small number of nonlinear elements [28,30,36].

4.2. Dynamic response prediction of clamped-clamped beam

Fig. 9 depicts the modal displacements and reconstructed displacement amplitudes for three excitation amplitudes in the frequency range around the lowest order resonance. The columns of Fig. 9 correspond to distinct excitation forces according to the amplitude scaling factor α that takes on a unit value in the column of Fig. 9(a,d). The modal forces applied to each DOF for $\alpha = 1$ correspond to a spatially uniform distributed load of 10 mPa. The results presented in Fig. 9 are generated for the use of the thermal load parameter $\Delta T = 4^{\circ}\mathbf{C}$, which is sufficient to buckle the clamped-clamped beam. The reconstructed displacement amplitudes given in the bottom row of Fig. 9 are generated for a location along the beam that is 40% from the clamped end at $x = 0$. At each frequency considered in Fig. 9, the analytical formulation is operated 96 times to identify the potential steady-state responses with high confidence. Numerical simulation facilitates a direct comparison of the displacement amplitudes predicted by the analysis, via an approximate solution to the governing equations, to the dynamic responses captured by directly numerically integrating the ROMs, and is therefore a valuable approach to verify the efficacy of

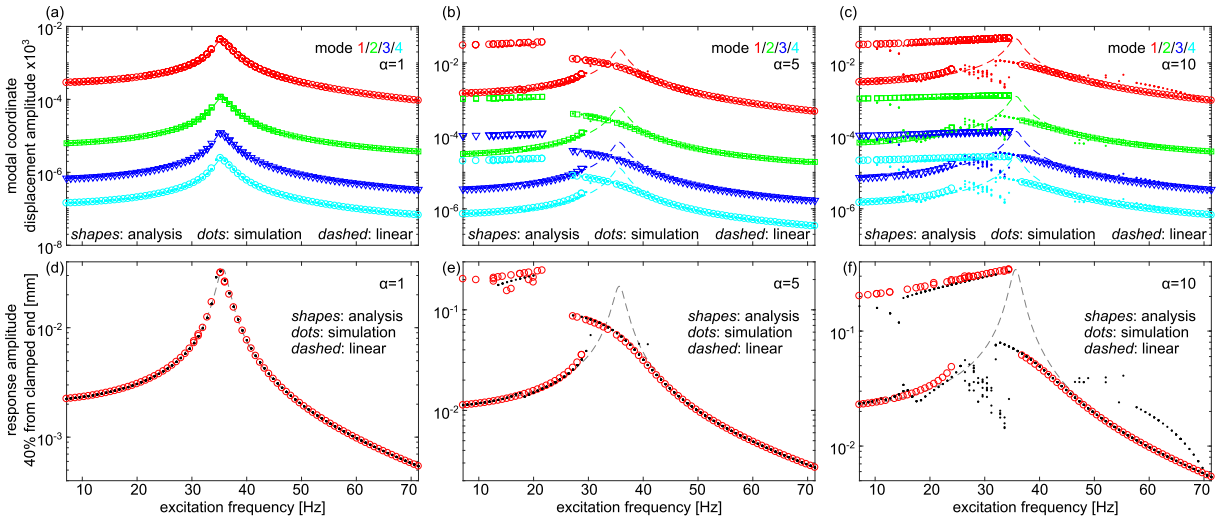

Fig. 9. Analytical and numerical frequency responses of a representative ROM with global nonlinear coupling around the first resonant peak. (a–c) Modal responses. (d–f) Reconstructed responses 40% from clamped beam end x = 0.

the analytical modeling efforts of Sec. 2.6. The simulations are generated via fourth-order Runge-Kutta numerical integration of the governing Eq. (37) over 250 excitation periods using 1024 time steps per excitation period. An FFT is then performed over the last 50 excitation periods to yield the response amplitudes shown by the simulation results of Fig. 9 as the dot data points. At each excitation frequency considered, the simulation is performed with 8 randomly generated sets of initial conditions.

Fig. 9(a,d) show the modal and reconstructed responses for $\alpha = 1$, respectively. Due to the relatively low amplitude of the excitation, a slight nonlinear softening of the resonant peak is predicted by both analysis (open markers) and simulation (dots). The modal and reconstructed analytical results (shapes) agree very well with simulation (dots), which do not ultimately deviate greatly from the underlying linear predictions (dash curves). For the case of $\alpha = 5$ shown in Fig. 9(b,e), the modal and reconstructed displacements demonstrate increased softening of the first resonance and emergence of large amplitude snap-through displacements for frequencies less than around 22 Hz. There is relatively good agreement in modal and reconstructed spaces between the numerical simulations and analytical predictions, despite such severe nonlinearity that richly couples the generalized coordinates of the 4-mode ROM.

Considering the higher forcing amplitude of $\alpha = 10$, the modal and reconstructed responses are shown in Fig. 9(c,f), respectively. The onset of aperiodic oscillations of the clamped-clamped and thermomechanically loaded beam is evident in the simulation results (dots) that occur in the bandwidth 20–35 Hz yet do not obtain consistent steady-state amplitudes of displacement. Giving attention to the steady-state behaviors, the analytical predictions of snap-through response are in close agreement with simulations. Likewise, analytical results for the lower amplitude intrawell oscillations at frequencies less than around 50 Hz are in good agreement with the numerical simulation. Yet, deviations between analytical and numerical results occur from 50 to 70 Hz in Fig. 9(f). For these excitation frequencies, the simulation predicts subharmonic oscillations at 1/3 and 1/2 orders in the frequency bands between 50-60 Hz and 60–70 Hz, respectively. The analysis, established on the assumption of a single periodic oscillation at the same frequency of the excitation, cannot predict the aperiodic or subharmonic oscillations and thus identifies no such behaviors in the nonlinear equation solution procedures. On the other hand, for the aperiodic simulation results with low amplitude in the frequency range around 20–35 Hz, the analysis indeed does *not* predict steady-state low amplitude behaviors, which is partial support to the presence of other-periodic motions. Moreover, the analysis predicts the snap-through dynamic regime with high fidelity, which is critical in many contexts of aerostructural systems operating in extreme environments.

In fact, the extended analytical framework achieves the response predictions for this 4-mode ROM using over two orders of magnitude less time than the simulations. The computational times for the analysis of the three cases shown in Fig. 9(a–c) are 0.0211, 0.0602, and 0.0573 s per attempt, respectively, which are 659, 231, and 227 times faster than the comparative simulation baselines. Thus, the analytical method originally proposed in Ref. [36] is broadly extended in this research to accurately model complex, coupled nonlinearities typical of myriad ROMs using a fraction of the computational time of numerical simulation.

The reconstruction of modal responses into the physical domain facilitates comparison to the exact time series generated via simulation. A comparison is made in Fig. 10 between coexistent (a) intrawell and (b) snap-through dynamic responses for $\alpha = 10$ at 21.6 Hz whose amplitudes are shown in Fig. 9(f). In Fig. 10, analytical results are denoted by solid blue curves while simulations are shown as red dash-dot curves. Higher-order harmonics are present in both intrawell and snap-through simulation responses, which leads to deviations in the shape of the simulated waveform with respect to the analytically predicted, single-harmonic response. Yet, the error between analysis and simulation remains low, specifically yielding RMS error of 0.13% and 7.3% for the intrawell and snap-through cases, respectively. In addition, the RMS error for peak-to-peak snap-through response is just 12%, thus yielding relatively accurate information for fatigue life predictions [52].

The newly established analytical framework is also observed to be well suited to predict higher order mode responses for the ROM. Fig. 11 depicts the (a) modal response and (b) reconstructed physical response near the second resonance at 360 Hz.

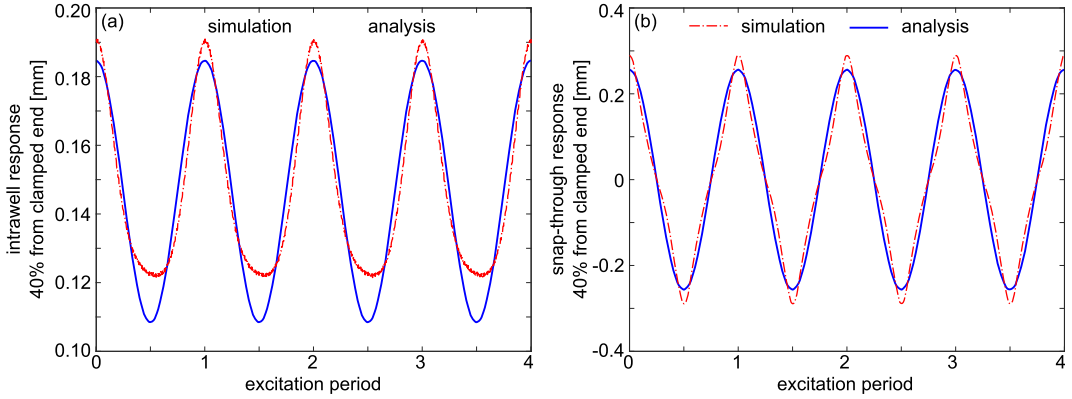

Fig. 10. Analytical and numerical time series at 21.6 Hz for $\alpha = 10$, reconstructed responses 40% from clamped beam end $x = 0$. (a) Intrawell dynamic responses. (b) Snap-through dynamic responses.

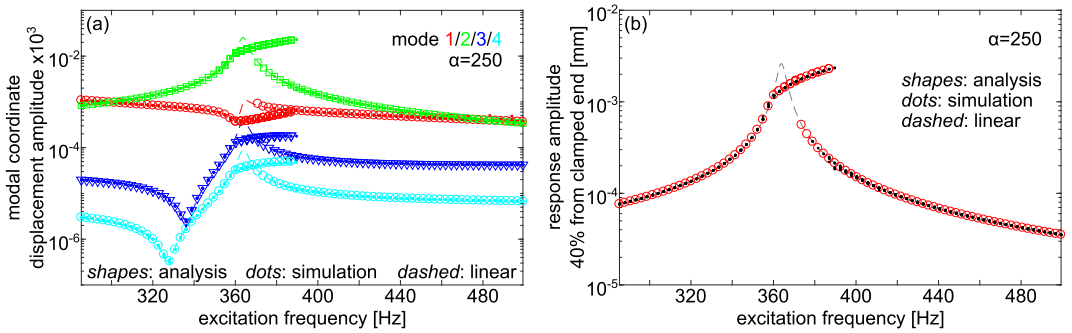

Fig. 11. Analytical and numerical frequency responses of a representative ROM with global nonlinear coupling around the second resonant peak. (a) Modal responses. (b) Reconstructed responses 40% from clamped beam end x = 0.

The excitation amplitude scaling factor is greatly increased to $\alpha = 250$ to more prominently trigger clear deviation from the underlying linear oscillations. The results of Fig. 11 plainly show that both modal and reconstructed displacements are accurately predicted by the analysis when compared to the more time-consuming simulations. Interestingly, both methods yield a cusp-like feature in the displacement amplitudes at a frequency slightly less than the second resonant frequency. The analysis captures this unique nonlinear dynamic well, in addition to the coexistent dynamic behavior and hardening resonance features suggested by simulation.

5. Conclusions

This research builds from an analytical framework to greatly enhance the capability to probe and characterize the harmonic forced dynamics of multistable structures. The enhancement encompasses four efforts: (i) normalization of the governing equations of motion, (ii) strategic initial guess seeding, (iii) establishment of an equivalent modal domain for new interpretation of the dynamic behaviors, and (iv) creation of an analytical formulation amenable to common nonlinearities and coupling manifest in myriad reduced order models (ROMs). For the case consisting of a three-DOF lumped parameter system with local nonlinearities and linear global coupling, the normalization and algorithmic enhancements lead to complete analytical predictions that uniquely facilitate the examination of coupled Duffing oscillators in the modal domain. The formulation of these equivalent nonlinear modes uncovers parallels between single-DOF bistable structures and the equivalent modal dynamics of multistable structures that warrant continued investigation for further deep, underlying ties. The utilization of the newly developed analysis for ROMs reveals the rich nonlinear response manifest in such systems that is previously inaccessible by other analytical techniques for nonlinear multi-DOF systems. By the establishment of the analytical formulation amenable to a wide variety of structural nonlinearities, this research delivers a predictive tool that may aid in the design and development of aerostructures operating in extreme, multi-physics loading environments where combinations of near-to- and far-from-equilibrium behaviors may be induced.

Acknowledgements

This research is supported in part by a U.S. Air Force Research Lab Summer Faculty Fellowship. B.A.G. acknowledges support from the U.S. Department of Defense Science, Mathematics, and Research for Transformation (SMART) Scholarship. The authors acknowledge helpful conversations with S. Michael Spottswood and Joseph J. Hollkamp of the Structural Sciences Center, Air Force Research Lab.

Appendix

The complete set of structural and excitation parameters for the system examined in Fig. 1(a) are presented in Table 1 for reference.

Table 1
Parameters for the discrete system of Fig. 1(a).

Parameter	Value	Parameter	Value	Parameter	Value
m_1	15.0 g	m_2	15.0 g	m_3	15.0 g
c_1	98.0 mN s/m	c_2	9.88 mN s/m	c_3	60.4 mN s/m
p_1	1.56	p_2	0.969	p_3	0.772
k_{NL11}	116 MN/m^3	k_{NL22}	33.0 MN/m^3	k_{NL33}	55.2 MN/m^3
k_{11}	192 N/m	k_{22}	24.8 N/m	k_{33}	287 N/m
k_{12}	59.9 N/m	k_{13}	29.4 N/m	k_{23}	47.4 N/m
F_1	0.200 mN	F_2	0.200 mN	F_3	0.200 mN
ϕ_1	0 rad	ϕ_2	0 rad	ϕ_3	0 rad

References

[1] A.P. Kothari, D. Webber, Potential demand for orbital space tourism opportunities made available via reusable rocket and hypersonic architectures, in: AIAA Space 2010 Conference & Exposition, Anaheim, CA, 2010.
[2] R.J. Mack, A Supersonic Business-jet Concept Designed for Low Sonic Boom, Langley Research Center, Hampton, VA, 2003.
[3] S.M. Spottswood, T.G. Eason, R. Chona, A structural perspective on the challenges associated with analyzing a reusable hypersonic platform, in: Proceedings of the 11th International Conference on Recent Advancements on Structural Dynamics, Pisa, Italy, 2013, pp. 1–11.
[4] L. Lees, Laminar heat transfer over blunt-nosed bodies at hypersonic flight speeds, J. Jet Propuls. 26 (1956) 259–269.
[5] C. Bisagni, R. Vescovini, Analytical formulation for local buckling and post-buckling analysis of stiffened laminated panels, Thin-Walled Struct. 47 (2009) 318–334.
[6] R.D. Blevins, D. Bofilios, I. Holehouse, V.W. Hwa, M.D. Tratt, A.L. Laganelli, P. Pozefsky, M. Pierucci, Thermo-vibro-acoustic Loads and Fatigue of Hypersonic Flight Vehicle Structure, 2009. AFRL-RB-WP-TR-2009-3139.
[7] A. Przekop, S.A. Rizzi, A reduced order method for predicting high cycle fatigue of nonlinear structures, Comput. Struct. 84 (2006) 1606–1618.
[8] B.A. Miller, J.J. McNamara, Time-marching considerations for response prediction of structures in hypersonic flows, AIAA J. 53 (2015) 3028–3038.
[9] A.J. Culler, J.J. McNamara, Impact of fluid-thermal-structural coupling on response prediction of hypersonic skin panels, AIAA J. 49 (2011) 2393–2406.
[10] A.J. Culler, J.J. McNamara, Studies on fluid-thermal-structural coupling for aerothermoelasticity in hypersonic flow, AIAA J. 48 (2010) 1721–1738.
[11] B.A. Miller, J.J. McNamara, S.M. Spottswood, A.J. Culler, The impact of flow induced loads on snap-through behavior of acoustically excited, thermally buckled panels, J. Sound Vib. 330 (2011) 5736–5752.
[12] R. Wiebe, S.M. Spottswood, On the dimension of complex responses in nonlinear structural vibrations, J. Sound Vib. 373 (2016) 192–204.
[13] M.P. Mignolet, A. Przekop, S.A. Rizzi, S.M. Spottswood, A review of indirect/non-intrusive reduced order modeling of nonlinear geometric structures, J. Sound Vib. 332 (2013) 2437–2460.
[14] A. Matney, M.P. Mignolet, A.J. Culler, J.J. McNamara, S.M. Spottswood, Panel response prediction through reduced order models with applications to hypersonic aircraft, in: 56th AIAA/ASCE/AHS/ASC Structures, Structural Dynamics, and Materials Conference, Kissimmee, FL, 2015, p. 1630.
[15] I. Kovacic, M.J. Brennan (Eds.), The Duffing Equation: Nonlinear Oscillators and Their Behaviour, John Wiley & Sons, Chichester, 2011.
[16] A.H. Nayfeh, D.T. Mook, Nonlinear Oscillations, Wiley, Weinheim, 1995.
[17] J. He, Some asymptotic methods for strongly nonlinear equations, Int. J. Mod. Phys. B 20 (2006) 1141–1199.
[18] D. Shou, J. He, Application of parameter-expanding method to strongly nonlinear oscillators, Int. J. Nonlinear Sci. Numer. Stimul. 8 (2007) 121–124.
[19] T.A. Nofal, G.M. Ismail, S. Abdel-Khalek, Application of homotopy perturbation method and parameter expanding method to fractional van der pol damped nonlinear oscillator, J. Mod. Phys. 4 (2013) 1490–1494.
[20] R.E. Mickens, Truly Nonlinear Oscillations: Harmonic Balance, Parameter Expansions, Iteration, and Averaging Methods, World Scientific, Hackensack, New Jersey, 2010.
[21] R.L. Harne, K.W. Wang, A review of the recent research on vibration energy harvesting via bistable systems, Smart Mater. Struct. 22 (2013), 023001.
[22] Q. Dai, R.L. Harne, Investigation of direct current power delivery from nonlinear vibration energy harvesters under combined harmonic and stochastic excitations, J. Intell. Mater. Syst. Struct. (2017), https://doi.org/10.1177/1045389X17711788.
[23] L.N. Virgin, R.B. Davis, Vibration isolation using buckled struts, J. Sound Vib. 260 (2003) 965–973.
[24] R.L. Harne, K.W. Wang, Harnessing Bistable Structural Dynamics: for Vibration Control, Energy Harvesting and Sensing, John Wiley & Sons Ltd., Chichester, 2017.
[25] F. Mattioni, P.M. Weaver, M.I. Friswell, Multistable composite plates with piecewise variation of lay-up in the planform, Int. J. Solid Struct. 46 (2009) 151–164.
[26] A. Pirrera, D. Avitabile, P.M. Weaver, Bistable plates for morphing structures: a refined analytical approach with high-order polynomials, Int. J. Solid Struct. 47 (2010) 3412–3425.
[27] Ö. Tanrikulu, K. Bayindir, H.N. Özgüven, M. İmregün, Forced harmonic response analysis of nonlinear structures using describing functions, AIAA J. 20 (1993) 1313–1320.
[28] Y.H. Chong, M. Imregun, Coupling of non-linear substructures using variable modal parameters, Mech. Syst. Signal Process. 14 (2000) 731–746.
[29] H. Elizalde, M. Imregun, An explicit frequency response function formulation for multi-degree-of-freedom non-linear systems, Mech. Syst. Signal Process. 20 (2006) 1867–1882.
[30] T. Kalaycıoğlu, H.N. Özgüven, Nonlinear structural modification and nonlinear coupling, Mech. Syst. Signal Process. 46 (2014) 289–306.
[31] W. Szemplińska-Stupnicka, The modified single mode method in the investigations of the resonant vibrations of non-linear systems, J. Sound Vib. 64 (1979) 475–489.
[32] P.D. Spanos, Stochastic linearization in structural dynamics, Appl. Mech. Rev. 34 (1981) 1–8.
[33] S.A. Rizzi, A.A. Muravyov, Comparison of nonlinear random response using equivalent linearization and numerical simulation, in: Structural Dynamics: Recent Advances, Proceedings of the 7th International Conference, Southampton, England, 2000, pp. 833–846.
[34] A.A. Muravyov, S.A. Rizzi, Determination of nonlinear stiffness with application to random vibration of geometrically nonlinear structures, Comput. Struct. 81 (2003) 1513–1523.
[35] C. Mei, K. Abdel-Motagaly, R. Chen, Review of nonlinear panel flutter at supersonic and hypersonic speeds, Appl. Mech. Rev. 52 (1999) 321–332.
[36] R.L. Harne, B.A. Goodpaster, Impedance measures in analysis and characterization of multistable structures subjected to harmonic excitation, Mech. Syst. Signal Process. 98 (2018) 78–90.
[37] D.J. Inman, Engineering Vibration, Prentice Hall, Saddle River, New Jersey, 2001.
[38] W.Y. Tseng, J. Dugundji, Nonlinear vibrations of a buckled beam under harmonic excitation, J. Appl. Mech. 38 (2) (1971) 467–476.
[39] R. Perez, X.Q. Wang, M.P. Mignolet, Nonlinear reduced-order models for thermoelastodynamic response of isotropic and functionally graded panels, AIAA J. 49 (2011) 630–641.
[40] P.T.D. Spanos, W.D. Iwan, On the existence and uniqueness of solutions generated by equivalent linearization, Int. J. Non Lin. Mech. 13 (1978) 71–78.
[41] R.L. Harne, Q. Dai, Characterizing the robustness and susceptibility of steady-state dynamics in post-buckled structures to stochastic perturbations, J. Sound Vib. 395 (2017) 258–271.
[42] I. Kovacic, M.J. Brennan, B. Lineton, On the resonance response of an asymmetric Duffing oscillator, Int. J. Non Lin. Mech. 43 (2008) 858–867.
[43] H.R. Elizalde Siller, Non-linear Modal Analysis Methods for Engineering Structures, Ph.D. dissertation, Imperial College London, London, 2004.
[44] D.H. Hodges, Proper definition of curvature in nonlinear beam kinematics, AIAA J. 22 (1984) 1825–1827.
[45] L.N. Virgin, Vibration of Axially Loaded Structures, Cambridge University Press, Cambridge, 2007.
[46] J. Lee, Large-amplitude plate vibration in an elevated thermal environment, Appl. Mech. Rev. 46 (1993) S242–S254.
[47] J.R. Dormand, P.J. Prince, A family of embedded Runge-Kutta formulae, J. Comput. Appl. Math. 6 (1980) 19–26.
[48] Y.L. Yeh, Chaotic and bifurcation dynamic behavior of a simply supported rectangular orthotropic plate with thermo-mechanical coupling, Chaos, Solit. Fractals 24 (2005) 1243–1255.
[49] J.V. Ferreira, Dynamic Response Analysis of Structures with Nonlinear Components, Ph.D. dissertation, Imperial College London, London, 1998.
[50] W. Szemplińska-Stupnicka, Bifurcations of harmonic solution leading to chaotic motion in the softening type duffing's oscillator, Int. J. Non Lin. Mech. 23 (1988) 257–277.
[51] R. Vaicaitis, Nonlinear response and sonic fatigue of National Aerospace Space Plane surface panels, J. Aircraft 31 (1994) 10–18.
[52] A. Przekop, S.A. Rizzi, K.A. Sweitzer, An investigation of high-cycle fatigue models for metallic structures exhibiting snap-through response, Int. J. Fatig. 30 (2008) 1579–1598.
[53] J.J. Hollkamp, R.W. Gordon, S.M. Spottswood, Nonlinear modal methods for sonic fatigue response prediction: a comparison of methods, J. Sound Vib. 284 (2005) 1145–1163.